Direct observation of beam impedance above cutoff

S. L. Kramer*

Brookhaven National Laboratory, National Synchrotron Light Source, Building 725C, Upton, New York 11973

(Received 4 September 2002; published 7 November 2002)

Measurements of microwave emission from an electron beam have shown signals below the shielding cutoff frequency of the beam pipe for coherent synchrotron radiation. The frequency spectrum of the signal below this cutoff frequency agrees with calculations and bench measurements of the impedance of a vacuum component in the ring. The wake fields produced in this impedance are above the waveguide cutoff frequency of the beam chamber, allowing the fields to propagate around the ring and out a photon beam port. Data are presented that rule out the possibility that this signal is coherent synchrotron radiation. This unique method of measuring propagating fields is discussed along with its application to measuring high frequency impedances and their impact on beam properties.

DOI: 10.1103/PhysRevSTAB.5.112001 PACS numbers: 29.20.-c, 29.27.-a

I. INTRODUCTION

Several synchrotron light sources have recently shown large power bursts in the microwave to far-infrared radiation (FIR) spectra from the beam [1]. Most of these signals appear to be coherent synchrotron radiation (CSR) emission above a current threshold that agrees in general with the microwave instability current threshold, I_t. This instability is due to high frequency fields induced in the vacuum chamber impedance by the beam. This beam impedance is difficult to calculate or measure accurately, partly due to the fact that fields of an isolated vacuum component, at these frequencies, can propagate freely around the ring through the beam chamber. Therefore, calculating or measuring the impedance of isolated components and summing their impedance may not be adequate above the waveguide cutoff. This uncertainty in estimating the beam impedance of the real vacuum chamber makes quantitative predictions of the beam properties difficult.

The VUV ring at the National Synchrotron Light Source has seen similar, high power bursts of radiation in the FIR and microwave spectrum [2]. These were first observed as annoying power bursts in the FIR spectra that saturated user's detectors in beam lines that allowed the propagation of this long wavelength synchrotron radiation. Consequently a program was started to study the source of these power bursts and the possibility of avoiding them. It was also considered that if this high power emission could be controlled that it might provide a stable high intensity source of FIR in the 100 GHz to multi-THz spectral range. While pursuing these measurements, a fortuitous cancellation of the synchrotron radiation spectra allowed measurements of the propagating high frequency, wake fields that are related to these power bursts. The results presented here have led to the possibility of a new method for measuring these fields *in situ* that could help address issues of high current beam instability in the actual vacuum chamber of synchrotrons.

II. EXPERIMENTAL METHOD

The VUV ring has a major commitment to FIR research, with four beam ports feeding six beam lines dedicated to this spectral range. Since the wavelength in these beams is so great, a large vertical and a horizontal beam aperture is necessary to provide adequate intensity. Two of these beam ports utilize the entire vertical aperture (42 mm) of the dipole chamber, by placing a water-cooled mirror immediately downstream of the dipole magnet. This mirror accepts 90×90 mrad of dipole synchrotron radiation, deflecting it vertically inside a >150 mm inner diameter vacuum pipe. Subsequent large aperture mirrors deflect and focus the FIR beam into an optical beam pipe, which directs the beam to one or more FIR spectrometers, Fig. 1. This beam pipe has a cutoff frequency of about 30 GHz, which prevents measurements below that frequency using the FIR spectrometers. However, a metal shutter was installed ahead of the optical beam pipe, which can be rotated to deflect a long wavelength beam through a glass viewport into air. The cutoff frequency of the beam pipe through the viewport is less than that of the dipole chamber itself. The rectangular dipole vacuum chamber has waveguide cutoff frequencies of $f \sim 1.87$ GHz for the $TE_{1,0}$ mode, $f \sim 3.64$ GHz for $TE_{0,1}$, and $f \sim 4.01$ GHz for $TM_{1,1}$.

The microwave emission from the electron beam was measured over a frequency range of 3 to 75 GHz, using seven different waveguide bands. The radiation transmitted through the viewport was collected using rectangular horn antennas coupled to standard rectangular microwave waveguides. A length of waveguide (at least six attenuation lengths) was used to filter out frequencies below the $TE_{1,0}$ cutoff for each waveguide. In four of the waveguides (centered on the peak signals), low pass filters were also used to prevent modes other than $TE_{1,0}$ from being detected. These filters attenuated signals with frequencies greater than the cutoff frequency of the next higher order waveguide modes (e.g., the $TE_{0,1}$ mode). This

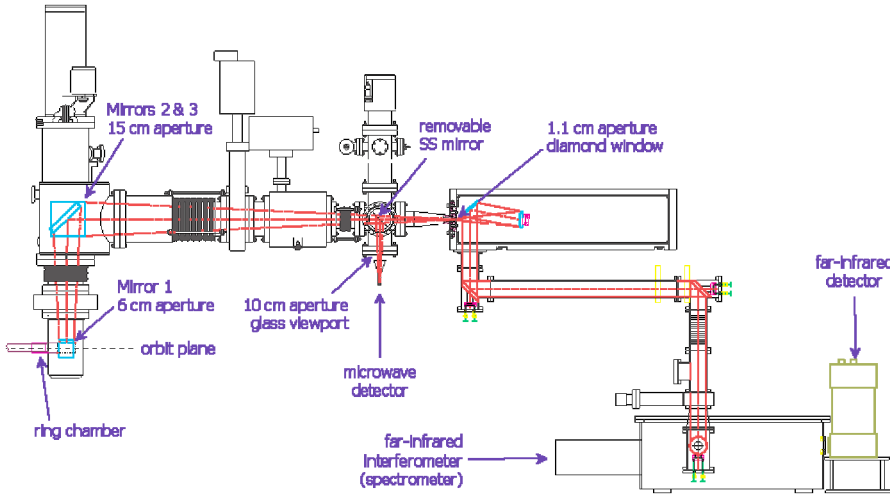

FIG. 1. (Color) Schematic layout of the U12IR beam line to the FIR spectrometer. The 1.1 cm diamond window and optical beam pipe are shown. Upstream of that window, a metal shutter (mirror) was inserted to deflect the microwaves through a viewport to a collector and detector.

provided essentially octave bands of microwave signal detection with negligible out of band signals and very low background noise levels. By limiting the waveguide signal to a single mode, only one polarization of E field was detected. Rotating the horn and waveguide allowed measurement of the linear polarization ratio of the detected radiation.

The microwave signal selected by each waveguide was detected using conventional rf detectors. Frequencies below 26.5 GHz were coupled to a coaxial cable using quarter wave stubs. Power in the band selected by the waveguide was measured with zero bias planar-doped or Schottky rf diode detectors (RDDs). Frequencies below 26.5 GHz used coaxial RDDs, while frequencies above that were measured by RDDs within the waveguides. The RDDs have a high sensitivity to rf power when terminated in high impedance, which limits their video bandwidth to $\sim$1 MHz. However, when terminated in 50 Ω the video bandwidth of the RDDs increases up to 1 GHz, but with considerably lower sensitivity. The latter termination will allow power signals from individual 50 MHz beam bunches to be measured. The output voltage for these detectors is linear in rf power only up to $\approx 100\ \mu$W. However, higher power bursts can be measured by attenuating the rf power with coaxial attenuators. This made accurate measurements of the peak power tedious and not possible above 26.5 GHz. This difficulty was overcome by measuring the average power in the selected band. Radio frequency diode power sensors (RDPSs) were used for power levels $\leq 3\ \mu$W (where the peak power typically is $\leq 100\ \mu$W) and rf thermocouple power sensors (RTPSs) for levels $\geq 0.1\ \mu$W. The RTPSs yield true average power to >100 mW, even for the large dynamic range and duty cycle variations of these microwave power bursts.

The power spectrum within each waveguide band was measured using conventional scanned microwave spectrum analyzers with scanned preselection filters ahead of the first rf mixer. This filter was essential for measurements of these signals, since image products at these frequencies are quite large. These false signals together with the pulsed nature of the real signals would fill the spectrum with pseudosignals making accurate spectrum measurements impossible. The preselection filters essentially eliminate the image products from the span of a measured spectrum, with a filter bandwidth greater than the rf resolution bandwidth. This allowed time characteristics of the temporal bursts to be measured to the limit of the rf resolution bandwidth ($\sim$2 MHz). All spectra were measured by storing the maximum signal detected at each frequency during >100 frequency scans, in order to sample adequately over the signal power bursts.

The measurements presented here were for a single bunch stored in the VUV ring at the injection energy of 737 MeV. Only the 52 MHz rf system was powered and the fourth harmonic rf system (used to stretch the bunch length in normal operations) was off and its cavity either shorted or detuned off resonance as far as possible. Measurements at other energies and rf conditions will be presented in a future publication.

III. MICROWAVE SIGNALS FROM THE BEAM

The power bursts of coherent FIR synchrotron radiation seen previously [2] showed the dominant signal came from a peak around 42 GHz with time between bursts of the order of $\sim$1 m sec. These power bursts occurred only when the bunch current exceeded a well-defined level ($I_t \approx 100$ mA at $E = 737$ MeV) that agrees with the microwave instability threshold, I_t, as determined by bunch

length measurements. Subsequent measurements showed that this peak was also observed as one of a series of interference peaks seen on the incoherent synchrotron radiation (ISR) spectrum and was the result of a reflection off the vacuum chamber outer wall [3]. These FIR measurements were limited to frequencies >30 GHz (described above). Figure 2 shows the measured microwave frequency spectrum over the range from 3 to 75 GHz, for beam currents ($I \sim 140$ to 210 mA) above I_t. This spectrum is the total of spectra from all seven waveguide bands, averaged over 0.5 GHz bins. This binning was essential since the rf spectral resolution is much smaller and shows considerably more detailed structure that may be difficult to separate from the temporal signals. These data show the maximum signal detected over the sampling time period and are plotted as the voltage into a 50 Ω load for a measured power level. Three peaks are clearly observed: A (5–8 GHz), B (20–28 GHz), and C (42–50 GHz). The term peak is used to avoid confusion with the microwave convention of labeling bands with letters. The peaks are really bands of peaks with some variations of the detailed structure with current (see below). The C peak agrees with that seen in the FIR spectra. The nature of the B and C peaks will be considered elsewhere [4], but basically they agree with CSR from the bunch when the current is above I_t. The A peak shows a serious disagreement with the cutoff frequency for CSR shielded by the vacuum chamber (see below).

To insure that these signals are from synchrotron radiation, the time structures of these signals were measured using wide bandwidth RDDs. Figure 3(a) shows the fast time domain signals for peaks B and C measured during a burst. Both of these signals are consistent with a prompt signal from a single bunch with the revolution time period spacing. The measured rise times for the B and C signals are 1.4 and 1.1 nsec, respectively. This is in agreement with the 500 MHz bandwidth of the scope, a bunch length $\sigma_t \approx 400$ psec, and a video bandwidth for the RDDs <1 GHz. The B signal RDD is a coaxial detector and is somewhat slower than the C signal RDD, which is within the waveguide. Figure 3(b) shows the time structure for the A and C signals, during a burst. The RDD used for the A signal was the same one used for band B, Fig. 3(a), and should see the same fast bunch signal. Surprisingly, the A signal shows a broad pulse with a FWHM of about 60 to 80 nsec and a peak displaced by >30 nsec after the bunch has passed the beam port. This signal cannot be from synchrotron radiation unless a mechanism, such as reflections, could account for this long time delay. It is just such a reflection that appears to be the source of the interference that creates the B and C peaks [3]. The delay time for that reflected ray is only 33 psec, while the 30 nsec delay of the A signal represents 20% of the ring circumference. Therefore, it is highly unlikely that synchrotron radiation could be the source of the A signal.

The large dynamic range of the power bursts makes quantitative peak power measurements difficult, therefore average power measurements were used for more

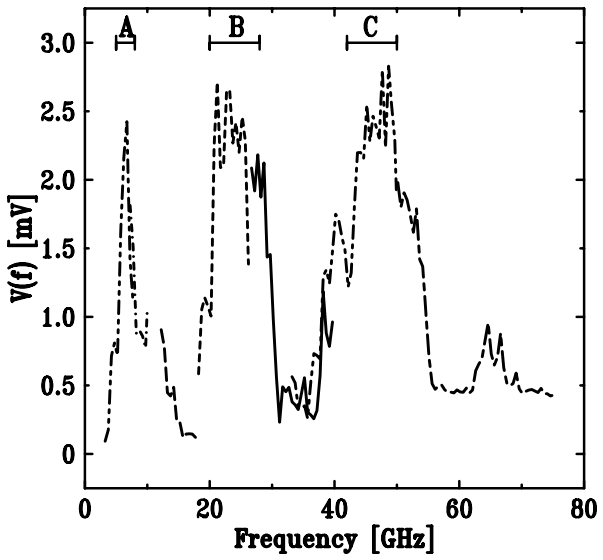

FIG. 2. The measured microwave spectrum for $I > I_t$. Different line dashing is used for each of the waveguide bands. The peaks labeled A, B, and C are described in the text.

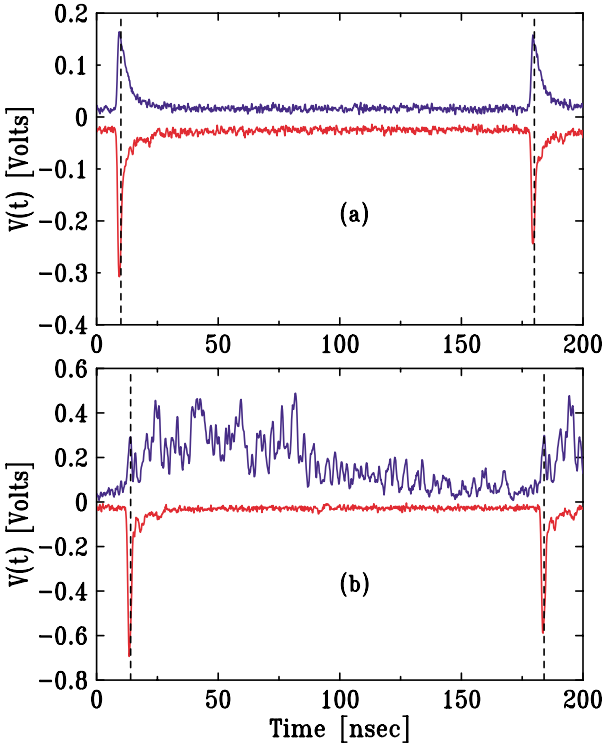

FIG. 3. (Color) Fast time structure for (a) B (positive, inverted signal) and C peaks and (b) A and C peaks. Vertical lines mark the revolution time for the single bunch.

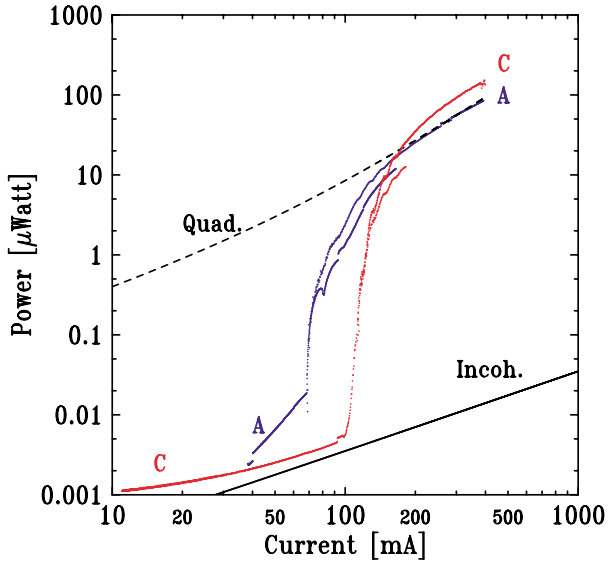

FIG. 4. (Color) Measured average power in A and C peaks versus bunch current. The curves show the calculated total ISR power (solid line) and a quadratic fit (dashed line) to the high current A peak data.

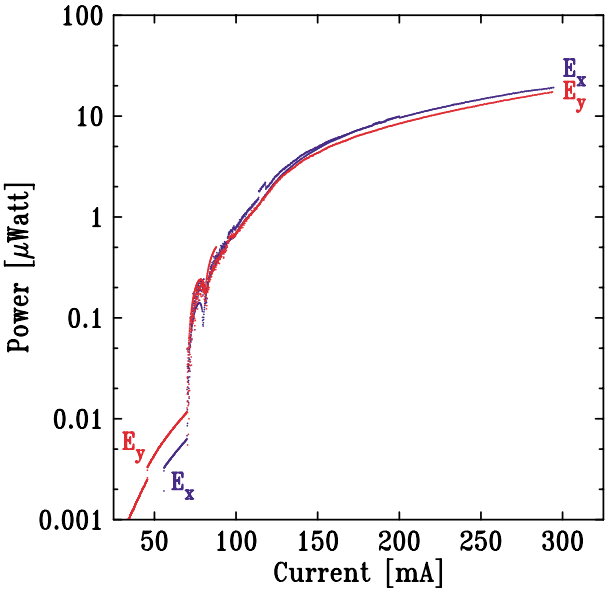

FIG. 5. (Color) The average power in A peak versus current for the two directions of linear E-field polarization of the collected radiation.

detailed comparison of these signals. Figure 4 shows the average power data (both RDPS and RTPS data are shown) for the band A and C peaks versus bunch current. The two power detectors agree quite well between 0.03 and 0.3 μW levels. Above this power level the nonlinearity (due to the high peak power of the bursts) of the RDPS measurements are obvious where they underestimate the total power, compared to the RTPS measurements. Although the A signal power increases almost 6 orders of magnitude from 10–400 mA, there is not a clear threshold at 100 mA, as there is in the C peak (similar for B). Also the A power never shows a linear dependence on the current, like the B and C signals show below I_t, indicative of ISR emission. The estimated total power for free space ISR emission in the A peak is also plotted in Fig. 4. The power level measured was significantly above this ISR power level for all currents above 10 mA, supporting the hypothesis that the A peak is not synchrotron radiation. A quadratic fit to the high current A power is also plotted in Fig. 4, which shows the coherent property of this radiation.

The on axis synchrotron radiation has a dominant linear polarization in the plane of the bend, E_x. As described above, the waveguide bands are designed to couple to only one direction of E-field polarization. This can be aligned with the dipole bend plane to yield power for E_x polarization. Rotating the collector and waveguide by 90° yields power measurements for the vertical polarization, E_y. Figure 5 shows the power level for both directions of polarization for the A peak signals. The measured power ratio E_x/E_y for the A peak varies from 1.3/1 at high current to 1/2 at 50 mA, compared to the ratio for the B and C peaks at high current of 36/1 and 106/1, respectively. This low value for the polarization ratio and its change with current for the A signal is contrary to what is expected for synchrotron radiation and what was observed for both the B and C peaks.

Detailed frequency measurements below 10 GHz are presented in Fig. 6(a). These data show that the peak of the power in this region shifts to lower frequencies for $I < I_t$. For $I > I_t$, the spectrum shows several peaks in the 6.7 GHz region. This frequency was confirmed by streak camera measurements of modulation of the bunch current distribution at 6.5 GHz, which was visible only during the A power bursts [5]. For $I < I_t$, the peak shifts to around 4.5 GHz indicating several resonances may be modulating the beam as the current changes. The streak camera has yet to confirm this shift in modulation frequency on the bunch. However, this shift of frequency signals was confirmed by measurements of the bunch current frequency spectrum using a beam position monitor (BPM) pickup signal, shown in Fig. 6(b). The low frequency part of the current spectrum grows to very large amplitudes and is clipped. The power at lower frequencies was so large that a 1 GHz high pass filter was necessary to avoid image products. The tail of the bunch current distribution is shown and displays less power bursts than the 4 to 8 GHz signals. The A peak signals are clearly observed as distinct peaks above the smooth bunch shape spectrum and the peak frequency varies with bunch current, similar to what was observed in Fig. 6(a). The two methods of diagnosing high frequency beam fluctuations shown in Figs. 6(a) and 6(b) can be compared. The microwave signal is larger for $I > I_t$ and does not require suppression of the low frequency tail of the bunch current signal. Average power

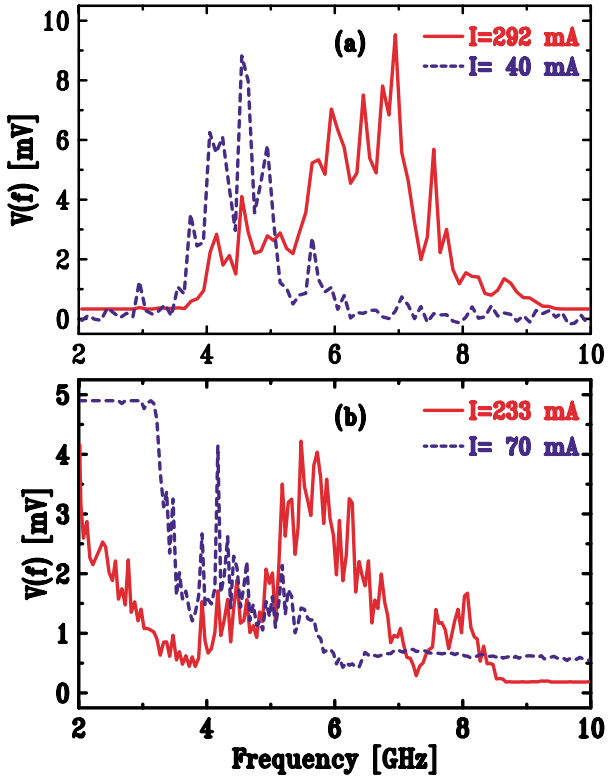

FIG. 6. (Color) Measured frequency spectrum for two values of bunch current: (a) microwave signal $I = 292$ and 40 mA (scaled by $220X$) and (b) bunch current signal $I = 233$ and 70 mA (scaled by $15X$).

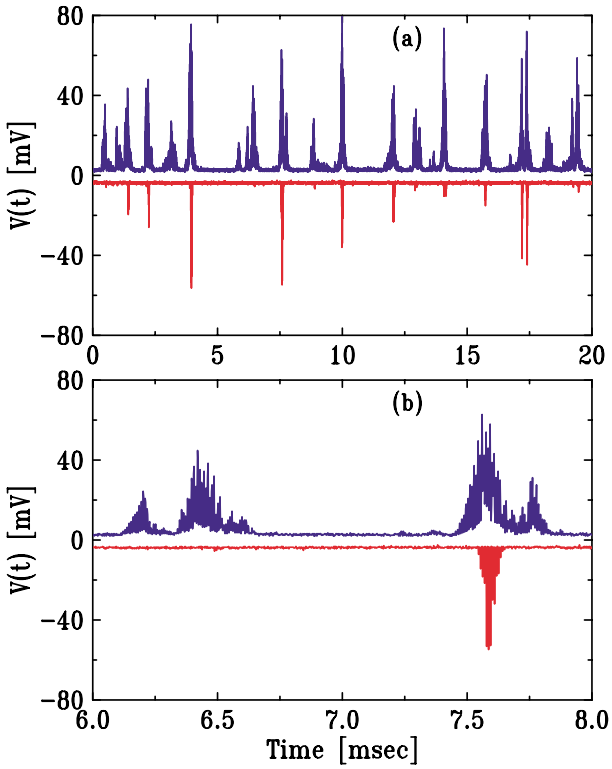

FIG. 7. (Color) (a) Peak A (positive) and C signals on a long time scale for $I > I_t$ and (b) detailed time structure of the power bursts.

measurements and high frequency amplifiers (shown below) extend the usefulness of the microwave detection technique to lower current. Also the microwave power can be detected outside the radiation shield of the accelerator, while the detector must be close to the BPM electrode for these frequencies.

In order to search for the source of these power bursts, the time intervals of the bursts for $I > I_t$ were measured and are shown in Fig. 7(a) for the A and C peaks. A time between bursts of $\sim$1 m sec is observed, with A always emitting before and sometimes without a C band emission. The A burst always lead the C burst and has a longer duration, Fig. 7(b). Between the bursts the signal drops to levels below the dynamic range of the scope. Since damping times are in the range of 5 to 10 msec, it is surprising that the signal reduction is so great between the bursts. With the microwave instability dominating the emission above I_t, a measurement of the time structure of the A peak below I_t was made. The collected A signal was amplified by 32 dB, with a 10 GHz amplifier prior to detection with the RDD and scope. This allowed measurements of the time and frequency structure of the signal to $I \sim 10$ mA. The fast time structure measured with the A signal below I_t is shown in Fig. 8(a). This time structure is almost identical to the signal measured without amplification above I_t, Fig. 3(b). However, the amplifier has a slower fall time for the bunch signal (non-dc coupled), resulting in a pulse pileup of the baseline. At a longer time scale in Fig. 8(b), the amplified A signal shows a similar time structure to the power bursts for $I > I_t$, as in Fig. 7(a), but with a smaller peak to valley ratio.

The frequency spectrum of the power bursts in the A peak shows many synchrotron frequency ($f_s \approx$ 11.1 kHz) harmonics out to 150 kHz, as shown in Fig. 9(b) for the measurement in Fig. 9(a). These oscillations appear to be the result of pulsed modulation on the rf cavity voltage, with a period shorter than the synchrotron radiation damping time. Above I_t, the microwave instability dominates the power levels being emitted from the beam and the damping between bursts. Below I_t, the synchrotron radiation damping does not reduce the signal between pulses as much, yielding power levels greater than expected for a stable bunch shape. This is shown in Fig. 10, where the A peak power was measured with the longitudinal damping system (LDS) turned on and off. The LDS suppresses synchrotron oscillations by increasing the damping rate for longitudinal dipole oscillations. Above I_t, the power in the A peak is independent of whether the LDS was on or off. Below I_t, the power level decreases by up to a factor of $2X$ with the LDS off. The ratio, LDS on to off, increases with energy and therefore the synchrotron radiation damping rate. This indicates

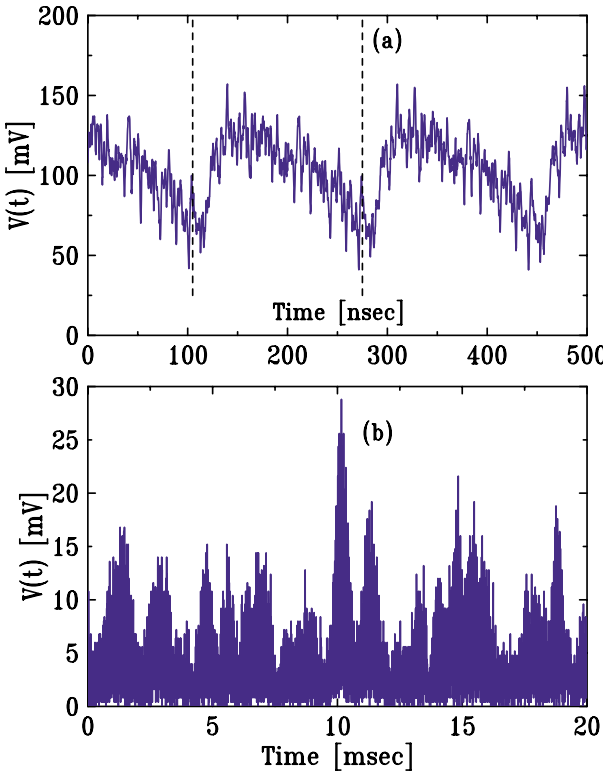

FIG. 8. (Color) The time structure of the amplified A peak signal for $I < I_t$. (a) Fast time interval for $I = 85$ mA and (b) slow time interval for $I = 26$ mA.

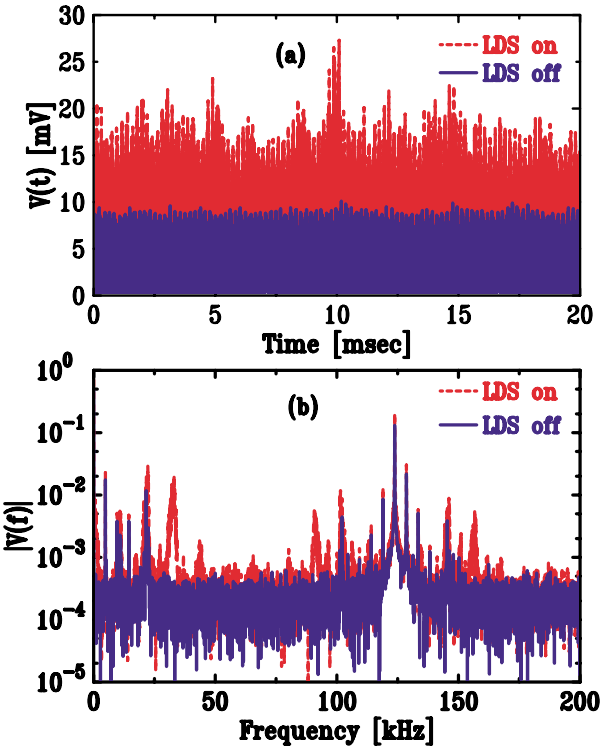

FIG. 9. (Color) (a) Amplified A peak signal for $I = 46$ mA with LDS on and off and (b) the frequency spectrum for these measurements.

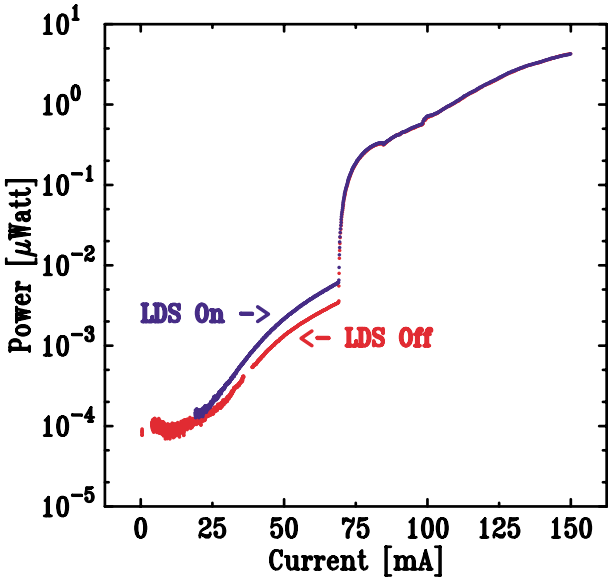

FIG. 10. (Color) The average power for the A peak versus bunch current at an energy of 737 MeV with the LDS turned on and off.

that the A signal is enhanced by bunch shape oscillations, since the LDS suppresses the dipole oscillation signal by 6 to 12 dB. Figure 9 shows that the increase in the A signal was due to an increase in the higher harmonics of the synchrotron frequency signals that are generated when the LDS is on.

IV. ANALYSIS OF THE A PEAK SIGNAL

When the large power bursts of the 42 GHz ($\lambda \approx 7$ mm) were first observed [2], a search was made for vacuum chamber components that might have a resonant frequency at this value. One component was identified, which had a periodic spacing of about 7 mm. This component was a copper rf shield for the vacuum chamber bellows. This shield was meant to reduce beam heating of the stainless steel bellows by the image currents of short bunches. This shield has ten convolutions with 7.2 mm spacing and a depth of 10 mm. There are a total of eight installed in the VUV ring, one at either end of the long straight section. Figure 11 shows the vertical half section of a shield, together with the bunch shape used to calculate the wake fields generated by the beam.

The impedance of bellows with convolution depth, Δ, has been studied by Lambertson and Ng [6], who characterized this impedance by a resonant mode with frequency, $f_r \approx c/(4\Delta)$ (i.e., $\Delta = \lambda/4$). For our shield, $\Delta = 1$ cm, this yields $f_r \approx 7.49$ GHz. However, a more detailed examination of the dependence on the beam pipe radius, b, gives a better approximation for the resonant frequency given by [6]

$$f_r \approx \frac{0.218c}{\Delta}\left[\frac{\Delta}{b}\right]^{0.052}. \quad (1)$$

This yields $f_r \approx 6.29$ GHz, which is closer to the

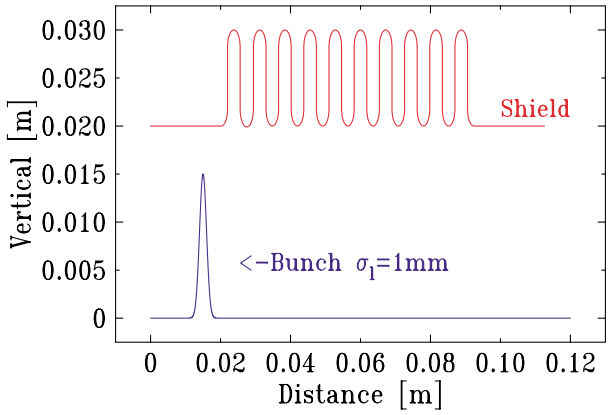

FIG. 11. (Color) Schematic of the vertical shape of shield for the VUV vacuum bellows and the bunch shape used for wake field calculations.

measured A signal and bunch current modulation frequency of 6.6 GHz. The above relations were derived for one convolution. As more convolutions were added, this resonant frequency was shown to decrease, making these estimates more in disagreement with the measured A signal for $I > I_t$.

The program ABCI [7] was used to calculate the wake field and potential induced by a short bunch ($\sigma_l = 1$ mm) passing through this rf shield. Since this program calculates only rotationally symmetric structures, we used the smaller vertical height of our rectangular shield to calculate these fields. The bunch was assumed to pass through the structure on or off axis and the wake potential was calculated for distances behind the bunch of up to 6 m. The wake potential was Fourier transformed to yield the beam impedance as a function of frequency. The impedances calculated for the cylindrical structure in Fig. 11 are shown in Fig. 12(a) for the monopole mode (azimuthally symmetric mode) $Z_{\parallel}(m = 0)$ and Fig. 12(b) for the dipole mode $Z_{\perp}(m = 1)$. The $Z_{\parallel}(m = 0)$ shows several peaks with maximums at 4.9, 5.55, and 6.25 GHz, while $Z_{\perp}(m = 1)$ shows a peak ~6.9 GHz. The latter is in better agreement with the measured frequencies, but raises a question of why the $m = 1$ impedance terms (driven by transverse offset of the bunch) might be the source of the measured propagating signal.

A calculation of the beam impedance for the 3D rectangular bellows was made using the new electromagnetic field solver GDFIDL code [8], using the same bunch length. The impedance was found for the longitudinal $Z_{\parallel}(0, 0)$ (beam centered) and the transverse $Z_x(0, 2)$ and $Z_y(0, 2)$ (beam displaced vertically 2 mm). These results are also presented in Figs. 12(a) and 12(b). In all three cases a sharp resonance is observed at 4 GHz, corresponding to the $TM_{1,1}$ waveguide cutoff frequency of our rectangular beam pipe. For the ABCI calculation the first TM mode is ~5.5 GHz and is embedded in the peaks around 6 GHz. The impedance peak at 6.2 GHz appears to be a broad

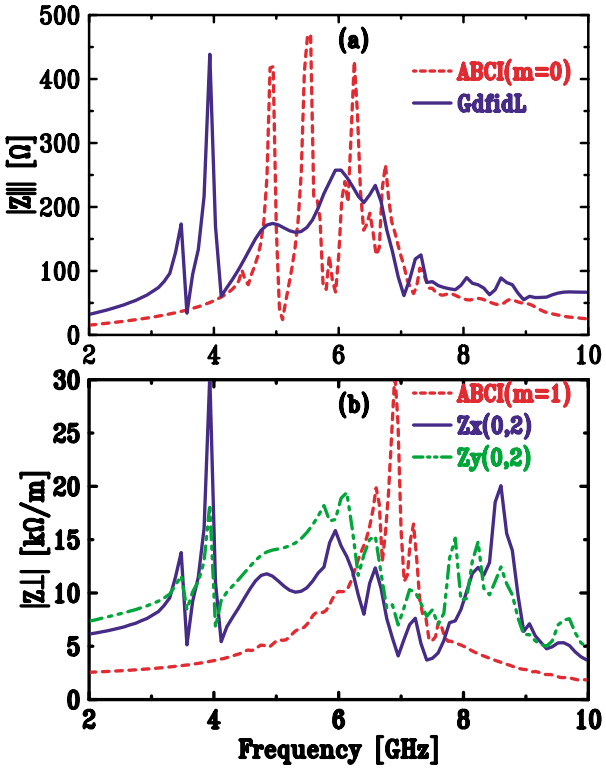

FIG. 12. (Color) (a) The longitudinal impedance calculated by ABCI, $Z_{\parallel}(m = 0)$ and GDFIDL, $Z_{\parallel}(0, 0)$ and (b) transverse impedance by ABCI, $Z_{\perp}(m = 1)$ and GDFIDL $Z_x(0, 2)$ and $Z_y(0, 2)$.

resonance, but this is partly the result of a lower frequency resolution for the GDFIDL calculation (wake potential calculated for <3 m displacement). Both Z_x and Z_y impedances show the 4 and 6.2 GHz peaks but also show a broad peak near 8 GHz. The latter peak is less obvious in the A signal, Fig. 6(a), but is clearly observed in the bunch current modulation signal, Fig. 6(b), at high current.

A section of the actual ring vacuum chamber was obtained, which contained the bellows shield, a slotted vacuum pump-out port and a four button beam position monitor. This bellow section and a reference chamber (straight section of the beam pipe without these components) were measured using both TEM and TM methods [9], using a 20 GHz network analyzer. Figure 13(a) shows the scatter parameter, $S_{2,1}$, for both beam pipe sections using a TEM drive (coaxial wire), with characteristic impedance of $Z_o \approx 235\ \Omega$. In order to avoid driving TM waveguide and cavity resonance modes, a tapered impedance transformation was used at both ends of the beam pipe sections. A microwave absorber was also used to suppress the TM modes [9]. $S_{2,1}$ for the bellows shield shows less signal coupling in the 4 to 8 GHz frequency region. The longitudinal beam impedance can be estimated [9] using the ratio of $S_{2,1}$ for the shield and the reference section

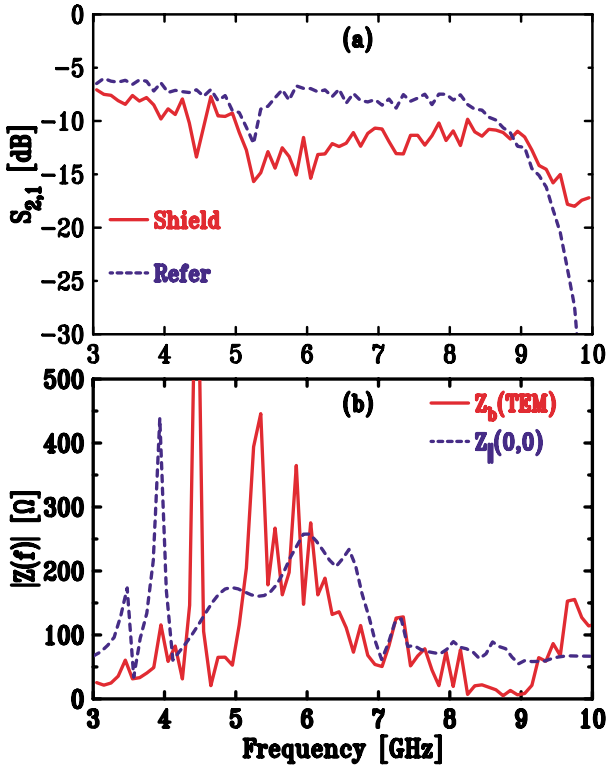

FIG. 13. (Color) (a) Measured $S_{2,1}$ for the TEM drive of the bellows shield and the reference section versus frequency and (b) the estimated beam impedance of the shield and the longitudinal impedance calculated by GDFIDL, $Z_{\parallel}(0, 0)$.

$$Z_b \cong 2Z_o\left[\frac{S_{2,1}(\text{ref})}{S_{2,1}(\text{shield})} - 1\right]. \qquad (2)$$

To the extent that the fields of the TEM drive are similar to those of an electron bunch, this impedance will be a reasonable estimate of the actual beam impedance. Figure 13(b) shows the estimated beam impedance for the measurement in Fig. 13(a) with a smooth curve fitted to $S_{2,1}$(ref). Also shown is the calculated $Z_{\parallel}(0, 0)$ from Fig. 12. The agreement is surprisingly good up to 9 GHz, except for a peak at 4.5 GHz. This peak may be the 4 GHz peak shifted by the presence of the wire or other components in the beam pipe. Above 9 GHz, the suppression of TM modes was not adequate to prevent cavity resonance in the reference section as well as the bellows shield, making measurements of the higher frequency impedance impossible with the present components. The structure and frequency of this impedance agrees better with the measured spectrum of the A peak for $I < I_t$, than for $I > I_t$, Fig. 6. The latter signal is peaked more above 6.5 GHz than the estimated impedance using the TEM drive.

The $TM_{1,1}$ waveguide mode can be used to probe the transverse impedance of the vacuum chamber. This mode was driven using the tapered transformers but with a $TM_{1,1}$ antenna [9] instead of the coaxial wire. The $S_{2,1}$ obtained with this method is shown in Fig. 14(a), for the bellows shield and the reference section. In this case the reference section shows a small attenuation at 6.6 GHz, which corresponds to the $TM_{3,1}$ waveguide cutoff frequency and cavity resonance for the vacuum chamber section. The bellows shield shows a much larger attenuation at and above this frequency. The beam impedance can be estimated for this mode using a similar relation to Eq. (2) and is shown in Fig. 14(b). There appears to be better agreement with the calculated impedance $Z_y(0, 2)$, above 6.5 GHz, but not below this frequency. The observed peaks around 8 GHz support the ABCI data that these higher frequency signals might be related to the transverse impedance of the shield. However, with several cavity modes being excited, the magnitude of the impedance estimates is less certain, but their peak frequencies should still be valid. In addition, many other vacuum components could be the source of these higher frequency signals.

The TM drive was also used to test the polarization measurements with the waveguide detectors. Placing the 4–8 GHz system downstream of the beam pipe with the TM drive showed the measured $S_{2,1}$ was independent of the direction of the E-field polarization selected by the

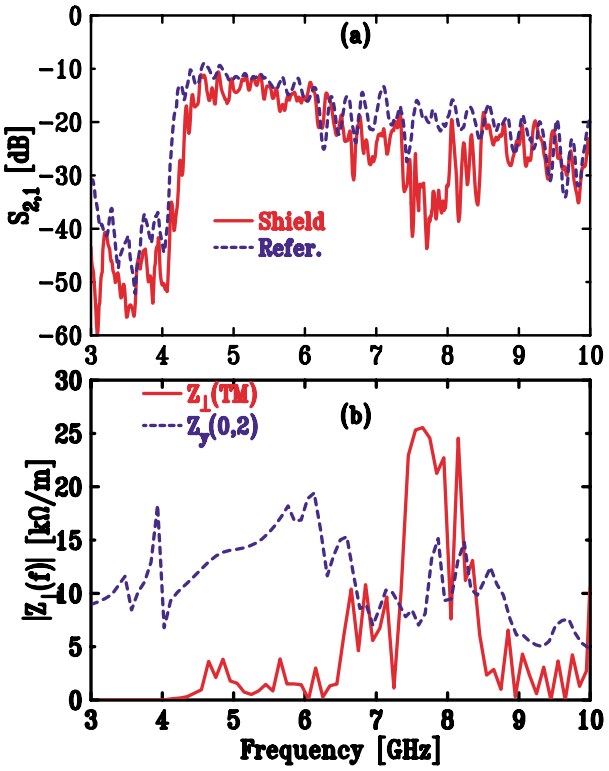

FIG. 14. (Color) (a) Measured $S_{2,1}$ for the TM waveguide drive of the bellows shield and the reference section versus frequency and (b) the estimated transverse beam impedance of the shield compared with the impedance calculated by GDFIDL, $Z_y(0, 2)$.

waveguide to <3 dB. This agrees with the measured polarization for the A peak.

These impedance estimates agree with the observed A peak being wake fields generated by the beam in the bellows shield, but they would be seen along with a prompt signal from the synchrotron radiation from the dipole. However, at these long wavelengths the synchrotron radiation field must also satisfy boundary conditions on the vacuum chamber metal surfaces. This effect has been calculated for the impedance due to CSR using a parallel plate model, for the upper and lower surfaces of the ring chamber [10]. It has been shown that this provides a shielding cutoff frequency [11]

$$f_c \approx \frac{c}{2}\sqrt{\frac{\rho}{h^3}}, \tag{3}$$

where ρ is the bend radius and h is the vacuum chamber full height. For the VUV dipole chamber $f_c \approx 24.1$ GHz, making the A peak and part of the B peak below f_c. Thus the ISR and CSR are extinguished by the existence of the beam chamber, allowing the wake fields from the bellows shield, which are above the waveguide cutoff frequency, to propagate around the vacuum chamber and out the FIR beam port. The presence of eight of these shields in the ring vacuum chamber, separated by curved dipole and straight chambers, could be the source of the dispersed signal seen in Fig. 3(b). The calculated wake fields ring for a long time following the passage of the bunch, but these calculations ignore the surface resistance of the vacuum chamber, which would damp the field faster. Work is in progress to try to model the dispersion of the wake field signal due to multiple separated shields.

The calculated beam impedance shows smaller peaks near 18 and 40 GHz, which could also propagate out the beam port. However, the presence of the large CSR or ISR signals in these regions would make it difficult to detect this signal. It is evident that the fields generated in this impedance would propagate in both directions around the beam pipe. Therefore reversing the direction of the mirror to accept a signal from the opposite direction to the beam, would block (absorb) both ISR and CSR and allow the generated wake fields to be observed. This study is being considered for the VUV ring, but the mechanical problems and user program disruption will be difficult to overcome, without important user advantages to these measurements.

V. CONCLUSION

We have directly measured, the wake fields induced by the electron beam in the vacuum chamber impedance of the ring, above the waveguide cutoff frequency of the beam pipe. These fields were detected using an existing large aperture FIR beam port, with standard microwave detectors. A band of signals (A peak) around 6.6 GHz appears to be largely the result of the impedance in the bellow shields. This signal, along with higher frequency signals, are observed to increase by 4 to 6 orders of magnitude above a threshold current. The higher frequency peaks appear consistent with CSR, while the A peak disagrees with the power resulting from synchrotron radiation based on the following measured properties.

(i) Below I_t, the intensity is too high for ISR, even ignoring the chamber shielding cutoff frequency.

(ii) The intensity dependence on current is never linear, as the ISR requires below I_t.

(iii) The time duration of the signal is not a prompt emission from the bunch, but is delayed from the bunch and has a duration equal to a significant fraction of the revolution time.

(iv) The polarization is not dominantly horizontal but the power is nearly equal for both directions.

(v) Below I_t the power level increases when the LDS suppresses the dipole mode oscillations while enhancing the higher order shape fluctuations of the beam.

The ability to see the A peak signal was shown to result from the vacuum chamber shielding cutoff frequency for synchrotron radiation. The measured spectrum of this signal shows significant agreement with the calculated and bench measurements of the impedance of the bellow shield in the ring. This microwave signal was shown to be a sensitive diagnostic for bunch shape fluctuations. The broad time duration of the measured fields will provide a new source of coupling for multiturn single bunch and coupled bunch instability calculations.

ACKNOWLEDGMENTS

This work was stimulated by the work of G. P. Williams and G. L. Carr, who have pioneered the FIR work on storage rings. This work benefited from many discussions with B. Podobedov and J. B. Murphy. I wish to gratefully acknowledge the help of W. Bruns with the 3D impedance calculations using his new program GDFIDL. This research has been supported by the U.S. Department of Energy.

*Email address: skramer@bnl.gov

[1] A. R. Hight-Walker *et al.*, Proc. SPIE Int. Soc. Opt. Eng. **3153**, 42 (1997); A. Andersson *et al.*, Proc. SPIE Int. Soc. Opt. Eng. **3775**, 77 (1999); M. Abo-Bakr *et al.*, in *Proceedings of the EPAC'00, Vienna* (European Physical Society, Geneva, 2000), p. 720.

[2] G. L. Carr *et al.*, Proc. SPIE Int. Soc. Opt. Eng. **3775**, 88 (1999); G. L. Carr *et al.*, Nucl. Instrum. Methods Phys. Res., Sect. A **463**, 387 (2001).

[3] G. L. Carr *et al.*, in *Proceedings of the PAC'01, Chicago* (IEEE, Piscataway, NJ, 2001), p. 377.

[4] S. L. Kramer and G. L. Carr (to be published).

[5] B. Podobedov *et al.*, in *Proceedings of the PAC'01, Chicago* (Ref. [3]), p. 1921.
[6] G. R. Lambertson and K. Y. Ng, Fermilab Report No. FN-487, 1988; K. Y. Ng, in *Proceedings of the PAC'87, Washington, DC* (IEEE, New York, 1987), p. 1051.
[7] Y. H. Chin, CERN Report No. CERN-SL/94-02(AP), 1994; O. Napoly *et al.*, Nucl. Instrum. Methods Phys. Res., Sect. A **334**, 255 (1993).
[8] W. Bruns, in *Proceedings of the EPAC 2002, Paris* (CERN, Geneva, 2002), p. 1619.
[9] G. R. Lambertson *et al.*, in *Proceedings of the EPAC'90, Nice* (Editions Frontieres, Gif-sur-Yvette Cedex, France, 1990), p. 1049.
[10] J. B. Murphy *et al.*, Part. Accel. **57**, 9 (1997).
[11] R. L. Warnock, in *Proceedings of the PAC'91, San Francisco* (IEEE, Piscataway, NJ, 1991), p. 1824.